Stochastic modelling of material variability in structural dynamics: A threefold comparison of Monte Carlo, polynomial chaos, and random sampling techniques

Rakesh Kumar*

*Department of Mechanical Engineering, Indian Institute of Technology Jodhpur,
NH 62, Surpura Bypass Street, Karwar - 342030, Jheepasani, Rajasthan, India*

Abstract:

This article investigates the influence of random elastic modulus on beam eigenfrequencies using multiple simulation techniques: Monte Carlo simulations (employing Cholesky decomposition (MCS-CD) and Kosambi-Karhunen-Loève expansion (MCS-KKL)), Polynomial Chaos expansion (PCE), and a proposed Random Sampling method (RSM). Anomalies in Monte Carlo simulations, where normally distributed elastic modulus led to negative values and imaginary eigenfrequencies, were effectively addressed by adopting a log-normal distribution. Comparative analyses focused on covariance variation of the first three eigenfrequencies with correlation length and standard deviation of the random field, highlighting nuanced differences between normal and log-normal distributions. PCE exhibited distinct responses, showcasing variations in covariance with different distributions. The study culminates in eigenfrequency estimation using the proposed RSM, wherein the beam is discretised into n elements with randomly assigned elastic moduli. The mean and variance of eigenfrequencies are compared with existing methods, which represent an alternative method for achieving similar outcomes. These comparative studies provide a comprehensive understanding of how different statistical treatments and simulation methods impact the reliability and accuracy of eigenfrequency predictions in beams with random elastic properties, thus contributing valuable insights for structural analysis and design under uncertainty.

Keywords: Kosambi-Karhunen-Loève expansion, Monte Carlo, polynomial chaos, probabilistic method, stochastic, vibration.

Classification number: 2.3

1. Introduction

Structural dynamics and vibration analysis are crucial aspects of engineering design, particularly when dealing with complex systems such as beams subjected to varying loads and uncertainties. In this context, the elastic modulus of materials plays a pivotal role in determining the response characteristics of structures. While traditional approaches often assume deterministic material properties, overlooking the intrinsic variability observed in real-world scenarios, Young's modulus has been reported to display randomness rather than consistency in various investigations [1-5].

In this article, the author investigates the impact of random elastic modulus on beam eigenfrequencies. The author analyses the consequences of using various simulation methods to better understand these effects. The investigation encompasses MCS with MCS-CD, MCS-KKL, PCE, and a proposed RSM. The primary focus is to unravel the nuances

associated with these methods and determine their efficacy in capturing the dynamic behaviour of beams subjected to uncertain elastic modulus distributions.

During simulations, it was observed that some elastic moduli were found to be negative in MCS with MCS-CD, leading to imaginary eigenfrequencies, particularly under certain conditions of normal distribution. The study unfolds by scrutinising this anomaly and reveals that transitioning to a log-normal distribution mitigates the issue. Comparative analyses of covariance structures between normal and log-normal distributions provide insights into the impact of distribution choice on the structural response.

Building upon this foundation, the article introduces MCS-KKL, showcasing similar negative modulus occurrences. The investigation culminates in an examination of eigenfrequency estimation using PCE and a proposed RSM. The latter involves discretising the beam into distinct
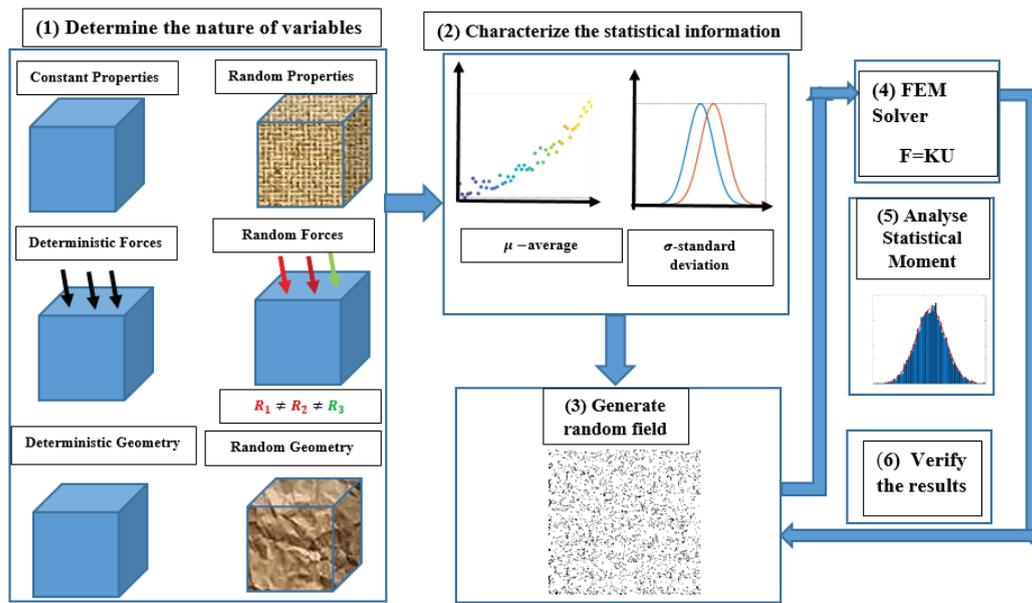
*Email: kumar.137@iitj.ac.in

Fig. 1. Schematic of random material and stochastic finite element method.

elements with randomly assigned elastic moduli, exploring a vast range of permutations to obtain a comprehensive understanding of the system's dynamic behaviour.

This research contributes not only to the fundamental understanding of how random elastic modulus influences beam eigenfrequency but also provides a comparative evaluation of simulation techniques. The insights gained herein are expected to advance the field of structural dynamics, guiding engineers and researchers towards more robust and accurate modelling approaches for systems subjected to material property uncertainties.

Figure 1 illustrates the adopted approach for structural analysis, incorporating randomness in material properties, loading, and geometry. The statistical properties of the structural response are inherently linked to the stochastic nature of the input parameters. Material properties, such as the elastic modulus, may exhibit spatial distribution and correlation across the structures. This necessitates a more comprehensive understanding of the probabilistic aspects of these parameters for robust structural design.

In literature, there are generally three methods for analysing how systems respond to random input variables. Firstly, perturbation methods [6-8] use Taylor series expansions, often truncated due to computational challenges. Secondly, polynomial chaos expansion [9, 10] relies on Hermite multivariate polynomials, evolving into Generalised Polynomial Chaos [11, 12]. Lastly, MCS directly computes responses for a large set of random inputs, estimating statistical indicators [13].

PCE efficiently represents system responses with random inputs. For instance, the elastic modulus can be represented by a random process, often exhibiting correlation between different points. The KKL decomposition is similar to Fourier expansion, expressing the random process as an infinite sum of orthogonal functions. This method can be truncated after a few terms [14-17]. The eigenvalues and eigenfunctions are obtained by solving Fredholm integral equations, with available closed-form solutions for some covariance functions [18]. Numerical methods, such as Galerkin and Nystrom methods, can be employed to solve these integral equations [16, 19].

The orthogonal polynomials obtained through KKL expansion form a basis for PCE, offering a concise representation of the stochastic system response. It represents a random variable using combinations of orthogonal polynomials. If system input parameters are random, the response is represented by a polynomial chaos expansion, minimizing errors through Galerkin projection.

Various researchers have proposed diverse methods to find eigenfrequencies, solving stochastic eigenvalue problems. Ghanem and Ghosh's approach provides a comprehensive probabilistic description of eigenvalues and eigenvectors using the Newton-Raphson algorithm [20]. Pascual and Adhikari introduced hybrid methods, like reduced spectral power and inverse power [21]. S.B. Mulani, et al. (2006) [22] presented a non-statistical eigenvalue extraction algorithm, demonstrating accuracy through generalised polynomial chaos. C.V. Verhoosel, et al. (2006)

[23] proposed a spectral expansion algorithm for random non-symmetric matrices, demonstrating efficient and robust performance. E. Sarrouy, et al. (2012) [24] utilised polynomial chaos expansion for complex eigenvalues and eigenvectors in damped structures.

P.C. Nguyen, et al. (2021) [4] used MCS, utilising finite element analysis and an iterative algorithm, to explore the natural frequencies of a beam on an elastic foundation with uncertain material characterised by a homogeneous Gaussian random field of elastic modulus, generated through the spectral representation method. The stochastic analysis of the FGM beam is conducted through MCS, in which elastic modulus and mass density are considered as one-dimensional homogeneous stochastic processes [25].

Cholesky decomposition factorises the covariance matrix into a product of an upper triangular matrix and its transpose '$\mathcal{L}$', where '$\mathcal{L}$' is lower triangular matrix. The lower triangular matrix $\mathcal{L}$ when applied to an uncorrelated vector u gives a sample vector $\mathcal{L}$ u having covariance properties as that of the modelled system.

2. Materials and methods

2.1. Monte Carlo simulation by Cholesky decomposition

In the present study, the vibration of a cantilever beam of length 'L' having variable elastic modulus 'E' along its length is considered. The elastic modulus of the beam is treated as a random property. It is assumed that the elastic modulus changes stochastically (with Gaussian distribution) and is a function of the location from one end of the beam. Therefore, one can represent the random variation of elastic modulus as [26]:

$$E(x)=E_0 [1+\alpha(x)] \tag{1}$$

where E_0 is mean value of the elastic modulus; $\alpha(x)$ is the level of randomness; and x indicates the position from the root of the beam. The expected mean of random variation is zero, i.e., $\mathbb{E}[\alpha(x)]=0$. Here, the symbol $\mathbb{E}$ represents the average value. Furthermore, the autocorrelation is defined as:

$$R_{\alpha\alpha}(\xi)=\mu[\alpha(x)\alpha(x+\xi)] \tag{2}$$

where ξ is the distance between two points x and $x+\xi$. This can extend to a 3-dimensional case using vector representation.

Considering this stochastic field as homogeneous and isotropic [27], the autocorrelation function of the spatial variation is a function of the distance $|\xi|$ only and is characterised by the variance σ_α^2. Thus, the autocorrelation function can be represented as:

$$R_{\alpha\alpha}(\xi) = \sigma_\alpha^2 \exp\left(-\frac{|\xi|}{d}\right) \tag{3}$$

where d is a correlation length that governs the rate at which the autocorrelation function decays. The standard deviation σ_α of $\alpha(x)$ represents the coefficient of variation (COV) of the elastic property of E(x). If the beam is divided into n elements (and assuming that each element has one specific value of elastic modulus), it will have n random values of homogeneous stochastic field $\alpha_i=\alpha(x_i)$; i=1, 2… n with mean zero, but are correlated. The correlation of elastic modulus between these n elements can be defined by a covariance matrix of size n×n. The covariance matrix, cov(αα), is defined as:

$$\text{cov}(\alpha\alpha)=\mathbb{E}[(\alpha-\mathbb{E}[\alpha]) (\alpha-\mathbb{E}[\alpha])^T] \tag{4}$$

$$=R_{\alpha\alpha}-\mathbb{E}[\alpha] \mathbb{E}[\alpha]^T \tag{5}$$

where $\mathbb{E}[\alpha]$ represents expectation.

Since, $\mathbb{E}[\alpha(x)]=0$, the correlation matrix $R_{\alpha\alpha}$ can be defined as $R_{\alpha\alpha}=\mathbb{E}[\alpha\alpha^T]$.

Therefore,

$$\text{cov}(\alpha_i\alpha_j)=R_{\alpha\alpha}(\xi_{ij})=\mathcal{L}\mathcal{L}^T \tag{6}$$

Now we can state

$$\alpha=[\mathcal{L}]Z \tag{7}$$

where vector $\{Z\}=\{Z_1, Z_2,… Z_N\}$ is an independent Gaussian stochastic vector with mean of zero and standard deviation of one, and $[\mathcal{L}]$ is a lower triangular matrix obtained from the Cholesky decomposition of the covariance matrix as in:

$$\mathbb{E}[\alpha\alpha^T] = \mathbb{E}[\mathcal{L}Z(\mathcal{L}Z)^T]$$
$$=E[\mathcal{L}(ZZ^T) \mathcal{L}^T]=\mathcal{L}\mathbb{E}[ZZ^T] \mathcal{L}^T \tag{8}$$

Now, $\mathbb{E}[ZZ^T]=1$, therefore:

$$\mathbb{E}[\alpha\alpha^T] = \mathcal{L}\mathcal{L}^T= \text{cov}(\alpha_i\alpha_j) \tag{9}$$

Figure 2 illustrates the variation of elastic modulus (E) with length for σ values of 0.3, 0.4, and 0.5, considering 50 realisations. It is evident that for σ=0.4 and σ=0.5, some elastic modulus values become negative, which is physically unrealistic and contradicts practical expectations. Additionally, with an increase in σ, the number of negative elastic modulus values rises. The literature recognises the challenge of encountering negative values post Cholesky decomposition of the random vector. It emphasises careful exclusion during simulations, particularly when significant variance exists in the random process, to ensure robust and reliable results [28].
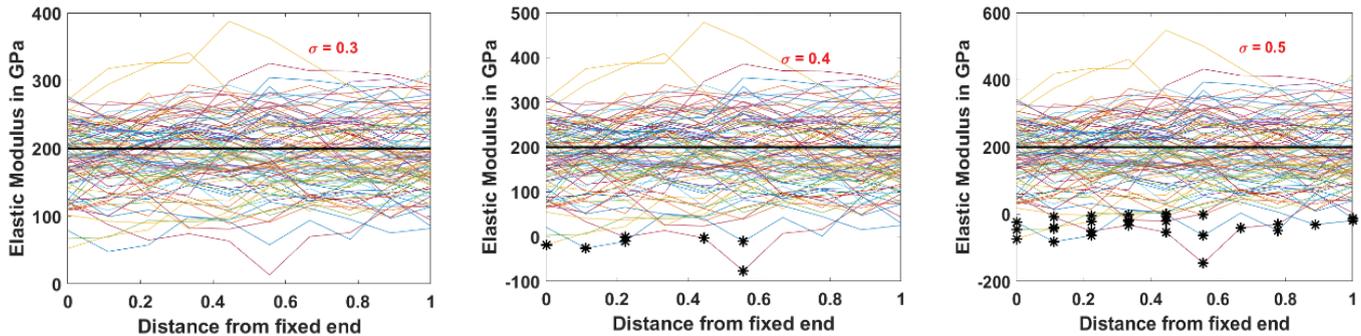
Fig. 2. Variation of elastic modulus with length (elastic modulus normally distributed).

It is crucial to acknowledge that the elastic modulus may exhibit negativity at any σ value due to our utilisation of a Gaussian normal distribution. To address this issue, we propose adopting a log-normal distribution for elastic modulus samples. This shift ensures the generated values remain strictly positive, aligning with physical expectations and resolving the observed problem.

To overcome the challenges encountered, we have integrated the log-normal transformation through the Cholesky decomposition method. Specifically, a vector of independent standard normal random variables, Z, is generated and transformed into correlated variables, α, using the lower triangular matrix L obtained from Cholesky decomposition as given in Eq. (7).

The transformation is expressed as:

$$\log\left(\frac{E}{E_0}\right) = \alpha \tag{10}$$

Here, $\alpha(x)$ represents the zero-mean random process capturing the random variation in elastic modulus, and the logarithmic transformation guarantees the strictly positive nature of the elastic modulus [29].

The impact of this log-normal transformation is depicted in Fig. 3, illustrating the variation of elastic modulus with length for different σ values (0.3, 0.4, and 0.5) based on 50 realisations. The results demonstrate that the adjustment effectively eliminates negative values of elastic modulus, ensuring that our model adheres more closely to physical expectations. As σ increases, the log-normal transformation prevents the occurrence of physically unrealistic negative values, providing more accurate and meaningful insights into the behaviour of elastic modulus in structures subjected to random mechanical fields.

In order to generate a Monte Carlo simulation, we need to determine the structural dynamic characteristics of the beam. The determination of structural dynamic characteristics of the beam using deterministic FEM is described as follows:
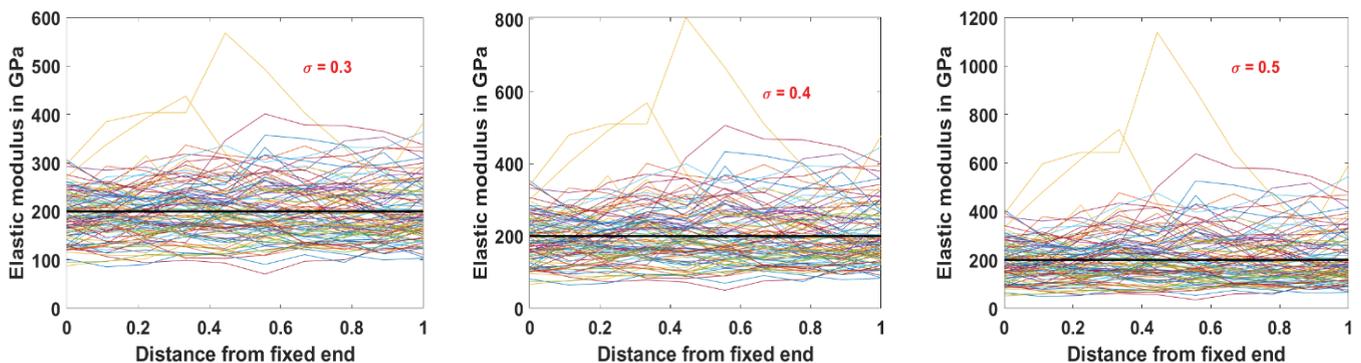

Fig. 3. Variation of elastic modulus with length (elastic modulus log normally distributed).

The Euler-Bernoulli equation for beam bending is

$$\rho\frac{\partial^2 v}{\partial t^2} + \frac{\partial^2}{\partial x^2}\left(EI\frac{\partial^2 v}{\partial x^2}\right) = q(x,t) \tag{11}$$

where $v(x,t)$ is the transverse displacement of the beam; ρ is mass density per volume; EI is the beam rigidity; $q(x,t)$ is the externally applied pressure loading; t is time; and x is spatial distance along the beam axis. The average weighted residual of Eq. (11) is:

$$\int_0^L \left\{\rho\frac{\partial^2 v}{\partial t^2} + \frac{\partial^2}{\partial x^2}\left(EI\frac{\partial^2 v}{\partial x^2}\right) - q(x,t)\right\} w\,dx = 0 \tag{12}$$

where L is the length of the beam; and w is test function. Galerkin's method is considered, where the test function is equal to the trial function.

The weak formulation is obtained from integrations by parts twice for the second term of the equation. In addition, discretisation of the beam into a number of finite elements gives

$$\sum_1^n \left[\int \rho\frac{\partial^2 v}{\partial t^2}w\,dx + \int EI\frac{\partial^2 v}{\partial x^2}\frac{\partial^2 w}{\partial x^2}dx - \int qw\,dx\right] + \left[Vw - M\frac{\partial w}{\partial x}\right]_0^L = 0 \tag{13}$$

The boundary conditions for the cantilever beam are as follows:

Displacement and slope are zero at x=0 i.e. $v(0)=w(0)=0$; $\theta = \frac{\partial v}{\partial x}_{(L=0)} = \frac{\partial w}{\partial x}_{(L=0)} = 0$ and Shear Force (V) and Moment (M) is zero at x=L.

Applying the boundary conditions, the last term of Eq. (13) becomes zero. Also, for free vibration, $q(x,t)=0$. Therefore, Eq. (13) becomes:

$$\sum_1^n \left[\int \rho\frac{\partial^2 v}{\partial t^2}w\,dx + \int EI\frac{\partial^2 v}{\partial x^2}\frac{\partial^2 w}{\partial x^2}dx\right] = 0 \tag{14}$$

There are four nodal variables for the beam elements, therefore, assuming a cubic polynomial function for $v(x)$:

$$v(x) = c_0 + c_1 x + c_2 x^2 + c_3 x^3 \tag{15}$$

Since an Euler-Bernoulli beam has been assumed, the slope is computed from Eq. (15) as $\theta=dv/dx$ where:

$$\theta(x) = c_1 + 2c_2 x + 3c_3 x^2 \tag{16}$$

Hermitian shape functions are applied:

$$v(x)=H_1(x)v_1+H_2(x)\theta_1+H_3(x)v_2+H_4(x)\theta_2$$

where

$$H_1(x) = 1 - \frac{3x^2}{l^2} + \frac{2x^3}{l^3}; \; H_2(x) = x - \frac{2x^2}{l} + \frac{2x^3}{l^2}; \; H_3(x) = \frac{3x^2}{l^2} - \frac{2x^3}{l^3}; \; H_4(x) = -\frac{x^2}{l} + \frac{x^3}{l^2}$$

Applying Hermitian shape functions and Galerkin's method to the second term of Eq. (14) we obtain the stiffness matrix of the beam element. Specifically,

$$[K]^e = \int_0^L [B]^T EI[B]\,dx \tag{17}$$

where $[B]=\{H_1'', H_2'', H_3'', H_3''\}$ and the corresponding element nodal degrees of freedom is $d^e=\{v_1, \theta_1, v_2, \theta_2\}^T$, and v_i and θ_i are deflection and slope nodal variables, respectively. The double prime denotes the second derivative of the function.

For dynamic analyses of beams, the transverse deflection is a function of x and t. The deflection is interpolated within a beam element as given below:

$$v(x) = H_1(x)v_1(t)+H_2(x)\theta_1(t)+H_3(x)v_2(t)+H_4(x)\theta_2(t)$$

The shape functions are used to interpolate the deflection in terms of the spatial domain and the nodal variables are functions of time. The first term in Eq. (14) becomes:

$$\int_0^L \rho A[H]^T[H]\{\ddot{v}\}\,dx \tag{18}$$

where $[H]=[H_1\ H_2\ H_3\ H_3]$ and the superscript dots denote time derivatives. From Eq. (18), the element mass matrix becomes:

$$[M^e] = \int_0^L \rho A[H]^T[H]\{\ddot{v}\}\,dx$$

The elemental stiffness and mass matrix are assembled to obtain global stiffness (K) and global mass matrix ($\mathcal{M}$). Thus, the equation of free vibration of beam becomes the Eigen value problem of the equation:

$$KX - \omega^2\mathcal{M}X = 0 \tag{19}$$

where ω is eigenfrequency. Making the substitution $\omega^2=\lambda$, the eigenfrequencies are obtained by finding the eigenvalue of the following equation:

$$(K - \lambda\mathcal{M})X = 0 \tag{20}$$

For MCS, the variations of elastic modulus (E) are generated using Eqs. (6), (7), and (1), which are substituted in Eq. (17). For each value of E, a corresponding eigenvalue and eigenvector can be obtained using Eq. (20). This procedure is repeated for a large number of random data sets of elastic moduli to produce an ensemble of the structural dynamic response characteristics. These values are used to compute the mean and standard deviation of the structural dynamic characteristics represented by the first three eigenfrequencies.

2.2. Kosambi - Karhunen - Loève expansion

In this method the cantilever beam of length 'L' having variable elastic modulus 'E' along its length is considered. The random field of elastic moduli has infinite-dimensional probability space (Ω,Θ,P), where Ω is set of elementary

events, Θ a sigma algebra generated on Ω, and P is a probability measure on (Ω,Θ). However, after the spatial discretisation, we have a finite dimensional representation of the random elastic field, which can be represented as a random vector:

$$x = [x_1, x_2 \ldots x_M]^T \tag{21}$$

where M can be regarded as the number of elements in a discretised model. So, for each x_i, i=1, 2… M is a random variable that represents the random elastic property in each element. The beam is discretised into M number of elements so that x_i is an M dimensional vector.

Now, assume we are given N number of realisations of the random elastic field $[x_1, x_2 \ldots x_N]$, where each realisation is represented as an M-dimensional column vector. The random vector x_i obtained after the discretisation are highly correlated. In order to obtain uncorrelated elastic moduli, we consider a nonlinear mapping φ that relates the input space R^M to another space F. We will refer to F as the feature space. These realisations x_i are mapped onto the feature space F to $\varphi(x_i)$, denoting the mean of the φ-mapped data by:

$$\bar{\varphi} = \frac{1}{N}\sum_{i=1}^{N}\varphi(x_i) \tag{22}$$

and defining the centred map as:

$$\tilde{\varphi} = \varphi(x) - \bar{\varphi} \tag{23}$$

The covariance matrix C in the feature space can be obtained as:

$$C = \frac{1}{N}\sum_{i=1}^{N}\tilde{\varphi}(x_i)\tilde{\varphi}(x_i)^T \tag{24}$$

The dimension of the covariance matrix is $N_F * N_F$ where N_F is the dimension of the feature space. The KKL expansion involves solving the eigenvalue problem CV=λV. As explained [30], N_F could be extremely large. As a result, it will be impossible to compute the C matrix and solve the eigenvalue problem directly. Thus, a kernel eigenvalue problem, which uses only dot products of vectors in the feature space, is formulated to solve the original eigenvalue problem indirectly [30]. The dot product in the feature space is defined as:

$$[\tilde{\varphi}(y_i).\tilde{\varphi}(y_i)] = \tilde{\varphi}(y_i)\tilde{\varphi}(y_i)^T \tag{25}$$

We now have to find eigenvalues $\lambda \geq 0$ and eigenvectors ϵ F such that CV=λV [31], which implies all solutions of V with $\lambda \neq 0$ lie in the span of $\varphi(x_1)$, $\varphi(x_2)$… $\varphi(x_N)$. For us, this has two useful consequences. First, we may instead consider the set of equations:

$$(\tilde{\varphi}(x_i)xCV) = \lambda(\tilde{\varphi}(x_i)xV), \forall i=1, 2 \ldots N \tag{26}$$

Second, there exist coefficients $\beta_j \forall$ j=1, 2… N such that we can expand the solution V as:

$$V = \sum_{j=1}^{N}\beta_j\tilde{\varphi}(x_j) \tag{27}$$

Now, combining Eq. (26) and Eq. (27), we obtain:

$$\frac{1}{N}\sum_{j=1}^{N}\beta_j\sum_{k=1}^{N}(\tilde{\varphi}(x_i).\tilde{\varphi}(x_k))(\tilde{\varphi}(x_k).\tilde{\varphi}(x_j)) \tag{28}$$

$$= \lambda\sum_{j=1}^{N}\alpha_j\tilde{\varphi}(x_i).\tilde{\varphi}(x_j)$$

for i = 1, 2… N

Defining the N*N kernel matrix R, which is the dot product of vectors in the feature space $\mathcal{F}$ R:R_{ij}= $\varphi(x_i).\varphi(x_j)$ and the corresponding centred kernel matrix:

$$\tilde{R}: \tilde{R_{ij}} = \tilde{\varphi}(x_i).\tilde{\varphi}(x_j) \tag{29}$$

We obtain $\tilde{R}^2\beta = N\lambda_i\tilde{R}\beta \forall$ i=1, 2… N

where $\beta = [\beta_1, \beta_2 \ldots \beta_N]$.

This is equivalent to the following kernel eigenvalue problem:

$$\tilde{R}\beta = N\lambda_i\beta \tag{30}$$

We rewrite above equation in the following matrix form:

$$\tilde{R}U = \Lambda U \tag{31}$$

where Λ=diag(λ_1, $\lambda_2 \ldots \lambda_N$) is the diagonal matrix of the corresponding eigenvalues, U = [β_1, $\beta_2 \ldots \beta_N$] is the matrix containing the eigenvectors of the Kernel matrix $\tilde{R}$, and each column consists of the ith eigenvector β_i = [β_1, $\beta_2 \ldots \beta_N$].

Therefore, through Eq. (27), the ith eigenvector of the covariance matrix C in the feature space can be shown to be [30, 32]:

$$\tilde{V}_i = \sum_{j=1}^{N}\tilde{\beta}_{ij}\tilde{\varphi}(x_j) \tag{32}$$

where $\tilde{\beta}_{ij} = \frac{\beta_{ij}}{\sqrt{\lambda_i}}$. It is easy to verify that Eq. (32) satisfies the orthonormal condition:

$$\tilde{V}_i.\tilde{V}_i = 1$$
$$\tilde{V}_i = \sum_{j=1}^{N}\beta_{ij}\sqrt{\lambda_i}\tilde{\varphi}(x_j) \tag{33}$$

Let x be a realisation of the random field with a mapping $\varphi(x)$ in $\mathcal{F}$. The random function $\varphi(x)$ can be decomposed in the following way:

$$\varphi(x) = \sum_{i}^{N}z_i\tilde{V}_i + \bar{\varphi} \tag{34}$$

where z_i is the projection coefficient onto the ith eigenvector $\tilde{V}_i$:

$$z_i = \widetilde{V}_i \cdot \widetilde{\varphi}(x) = \sum_{j=1}^{N} \tilde{\beta}_{ij} \tilde{\varphi}(x) \cdot \tilde{\varphi}(x_j) \tag{35}$$

Normalising the coefficient z_i as $\varepsilon_i = \frac{z_i}{\lambda_i^{1/2}}$ where ε_i are zero mean, mutually uncorrelated random variables with unit variance [32], we can represent $\varphi(x)$ as:

$$\varphi(x) = \sum_{i=1}^{N} \varepsilon_i \lambda_i^{1/2} \widetilde{V}_i + \overline{\varphi} \tag{36}$$

From Eq. (29), it can be seen that in order to compute the kernel matrix, only the dot products of vectors in the feature space F are required, while the explicit calculation of the map $\varphi(x)$ does not need to be known. As shown [33], the dot product can be computed through the use of the kernel function. Not all arbitrary functions except the Mercer kernels can be used as a kernel function [30]. The kernel function $R(x_i x_j)$ calculates the dot product in space F directly from the vectors of the input space $\mathbb{R}^M$. Mercer proved that any positive definite function $R(x_i, x_j)$ with x_i, $x_j \in \mathbb{R}^D$ defines an inner product of another vector space V. $R(x_i, x_j)$ is called the covariance or kernel function [34]. In this article, we have used exponential covariance function $R_{\alpha\alpha}(\xi) = \sigma_\alpha^2 \exp(-\frac{|\xi|}{d})$. Kernels depend on a parameter d called the correlation length, describing the correlation between two points of the field. The limit $d \rightarrow \infty$ generates a fully correlated random field, whereas $d \rightarrow 0$ produces a random field without any spatial correlation [35].

Since R is real and symmetric, it has an Eigen decomposition of the form:

$$R(s,t) = \sum_i \lambda_i V_i(s) V_i(t) \tag{37}$$

where λ_i are eigenvalues and V_i are eigenvectors of R.

The eigenvectors are obtained by solving the homogenous Fredholm integral equation of the second kind [36] as:

$$\int_a^b R(x,y) V_k(x) dx = \lambda_k V_k \tag{38}$$

Writing random functions as $\varphi(x,\theta) = E(x,\theta))$, $\overline{\varphi} = E_0$, and $\sum_{i=1}^{N} \varepsilon_i \lambda_i^{1/2} \widetilde{V}_i = E_0 * \alpha(x,\theta)$, we have:

$$E(x,\theta) = E_0[1 + \alpha(x,\theta)] \tag{39}$$

where $\mathbb{E}[E(x,\theta)] = E_0$ is the mean value of the random elastic field and $\alpha(x,\theta)$ is a zero mean random process.

Figure 4 shows the Mercer Eigen functions. Fig. 5 shows the realisations of the random function α having zero mean.
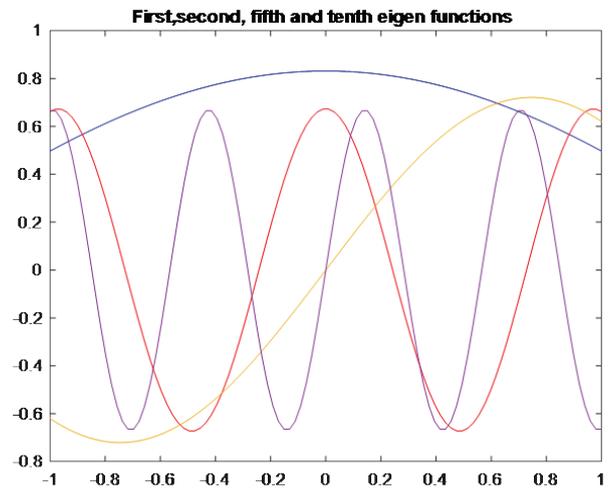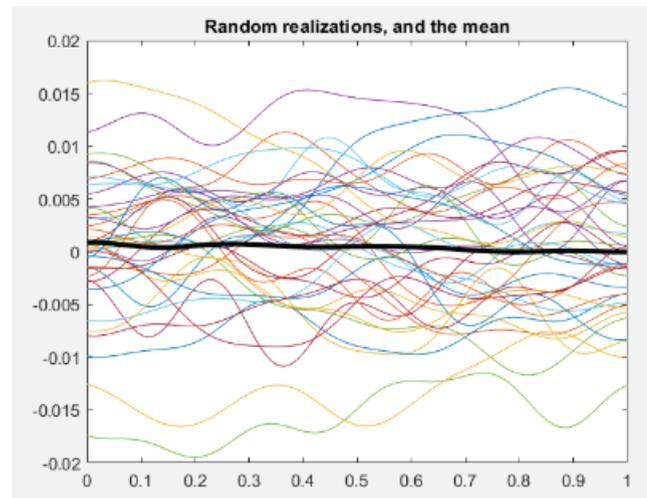

Fig. 4. Representation of eigenvalues.

Fig. 5. Realisations of random function alpha.

2.3. Truncation of Kosambi-Karhunen-Loève expansion

In order to obtain a random process, an infinite sum of linear combination of eigenfunction is not required. The series can be truncated after a finite number of terms, the specific value of which depends on the desired level of accuracy. The proof for truncation is explained below.

Random coefficients ξ_m of the KKL expansion are uncorrelated having zero mean and unit variance. The variance of α is simply the sum of the variances of the individual components of the sum:

$$var[E(x,\theta)] = var[E_0 * \alpha] = \sum_{k=1}^{N} \lambda_k V_k^2 var[\varepsilon_k] \tag{40}$$

Since var $[\xi_k] = 1$,

$$E_0{}^2 \text{var}[\alpha] = \sum_{k=1}^{N} \lambda_k V_k{}^2 \qquad (41)$$

Using the orthonormality of V_k, we obtain the total variance of the process:

$$E_0{}^2 \text{var}[\alpha] = \sum_{k=1}^{N} \lambda_k \qquad (42)$$

The total variance of the T-truncated approximation is given by the sum of the first T eigenvalues denoted as $\sum_{k=1}^{T} \lambda_k$. Consequently, the T-truncated expansion explains a proportion of the variance equal to $\frac{\sum_{k=1}^{T} \lambda_k}{\sum_{k=1}^{N} \lambda_k}$ of the variance.

For instance, if we seek an approximation that accounts for 95% of the variance, we must determine a value of T such that

$$\frac{\sum_{k=1}^{T} \lambda_k}{\sum_{k=1}^{N} \lambda_k} \geq 0.95 \qquad (43)$$

The truncation order 'T' obtained is 5 for 95% accuracy and 3 for 90% accuracy. Note that the statement "The truncation order 'T' obtained is 5 for 95% accuracy and 3 for 90% accuracy" indicates the level of approximation achieved through truncating the MCS-KKL. In essence, it means that by considering the first 5 terms in the expansion, we can capture 95% of the total variance of the process, while for 90% accuracy, only the first 3 terms are necessary. This is based on the fact that Eq. (42), the total variance of the process, can be represented as the sum of the eigenvalues associated with each term in the expansion. By truncating at a certain order, we essentially prioritise the dominant modes that contribute most to the variance of the process.
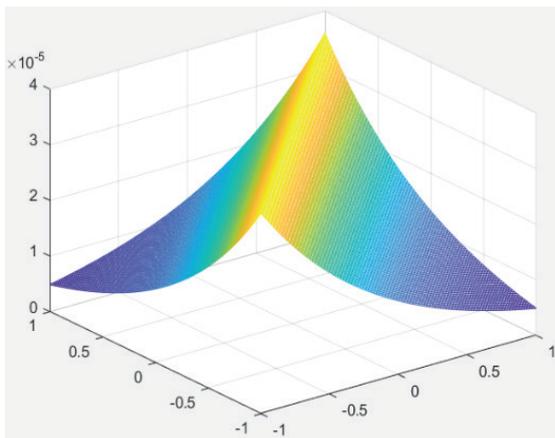

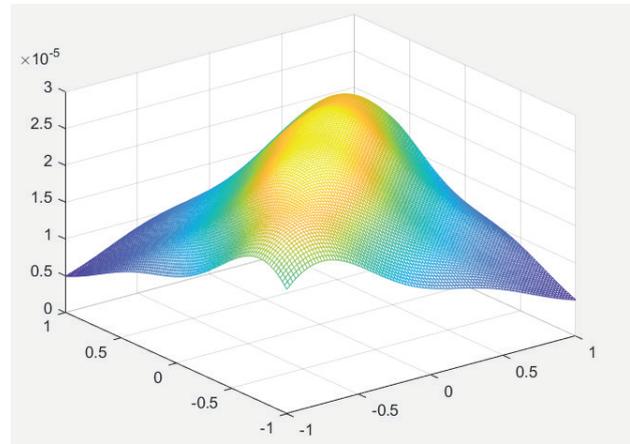Fig. 6. Bending stiffness covariance $R = \sigma^2 \exp\left(-\frac{|\xi|}{d}\right)$.

Fig. 7. Bending stiffness covariance for truncated Kosambi-Karhunen-Loève expansion of order T=5.

Figure 6 shows the bending stiffness covariance $R = \sigma^2 \exp(-\frac{|\xi|}{d})$ and Fig. 7 shows the bending stiffness covariance for a truncated KKL expansion of order T=5. Fig. 8A shows the realisation of alpha (zero mean random process) after a truncation order T=5. Fig. 8B, shows the bending stiffness in GPa after a truncation of the KKL expansion of order T=5.
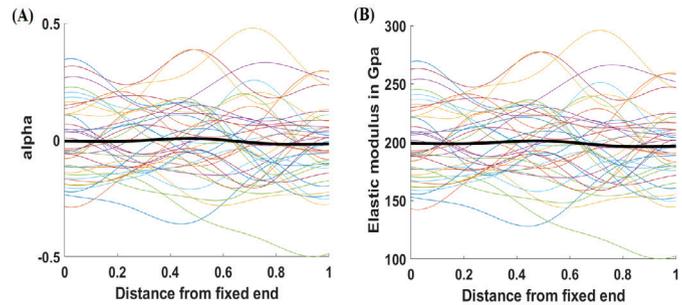

Fig. 8. Variation of elastic modulus with length for Kosambi-Karhunen-Loève expansion of truncation order 5.

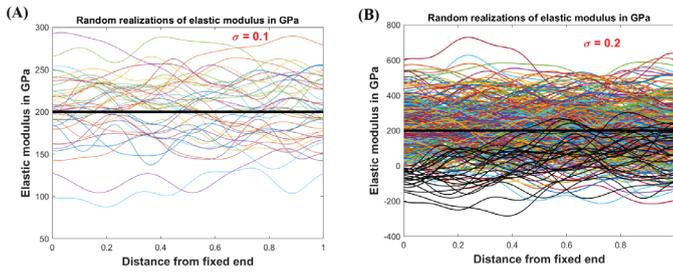The bending stiffness of the beam $K(x,\theta)$ is linearly dependent on a random process $E(x,\theta)$, i.e.,

$K(x,\theta)=K(E(x,\theta))$. Now $K(x,\theta)$ can be written as:

$$K(x, \theta) = \mathcal{K}(E(x, \theta)) \approx K_0 + \sum_{j=1}^{T} K_j \xi_j(\theta) \qquad (44)$$

where K_0 is the stiffness matrix of the mean system. The deterministic matrices K_j are given by the operator:

$$K_j = \begin{cases} \mathcal{K}(E_0) & j = 0 \\ \mathcal{K}\left(\sqrt{\lambda_j} V_j(x)\right) & j = 1 \dots T \end{cases} \qquad (45)$$

The bending stiffness for a given realisation can thus be calculated by Eq. (44).

Fig. 9. Variation of alpha and elastic modulus with length for normal distribution.

Figure 9A shows the realisation of elastic modulus with length for σ=0.1, while Fig. 9B displays the realisation of elastic modulus with length for σ=0.2. The black curve in Fig. 9B represents instances where the elastic modulus values are negative, which is physically impossible. To address this issue, the elastic modulus is considered as lognormal, and it is depicted in Figs. 10A and 10B for σ=0.1 and σ=0.2, respectively.
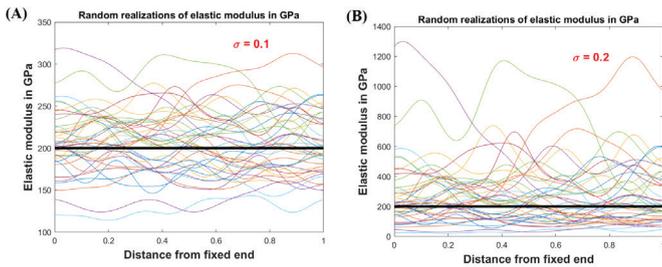
Fig. 10. Variation of alpha and elastic modulus with length for lognormal distribution.

In order to calculate MCS for KKL, the process is described as follows:

(i) Assemble the system matrices K_j.

(ii) Generate the sets of independent standard Gaussian variables $\{\xi_1(\theta_i),\dots \xi_T(\theta_i)\}$ with i=1,... n_{MCS}.

(iii) Assemble the stiffness matrix $K(\theta_i)$, for every realisation i.

(iv) The eigenfrequency is obtained by finding the eigenvalue of the equation

$$KX = \omega^2 \mathcal{M}X = (K - \lambda\mathcal{M})X = 0 \qquad (46)$$

(v) Solve the deterministic system of equations $K(\theta_i) X = \lambda\mathcal{M}X$.

The mean and variance of MCS obtained after KKL decomposition converges nearly after 1500 samples as shown in Fig. 11. For calculation purposes, the number of MCS is taken as 2000.

2.4. Polynomial chaos expansion

In the polynomial chaos method, the solution u(θ) of differential equations are projected on a vector space spanned by polynomials $\psi_i(\xi)$. In this article, we discuss the Galerkin-based intrusive spectral projection method. In this approach, a random variable is represented as spectral representation in terms of a set of polynomial basis functions:

$$u(\theta) = \sum_{i\in\mathbb{N}} u_i \psi_i(\xi) \qquad (47)$$
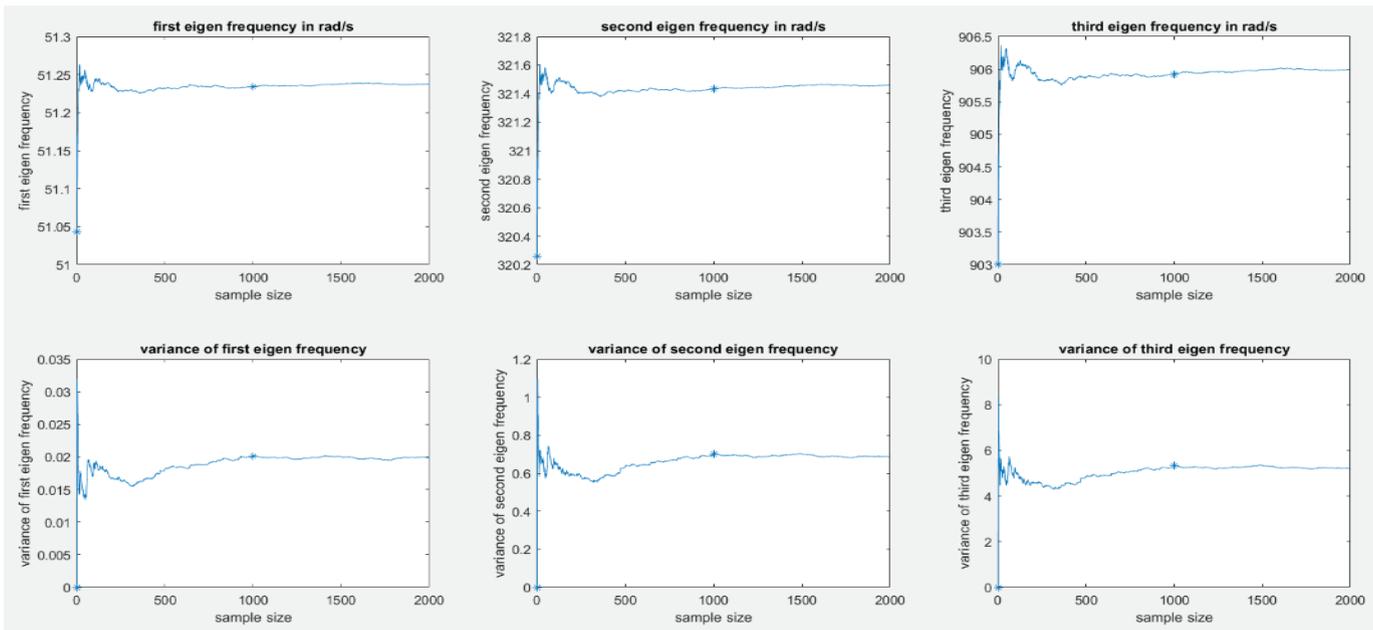
Fig. 11. Mean and variance of the first three eigenfrequencies of Monte Carlo simulation obtained after Kosambi-Karhunen-Loève expansion decomposition having truncation order 'T'=5.

where $u(\theta)$ is a random variable and $\psi_i(\xi)$ is a polynomial function of another random variable ξ.

The polynomials are chosen to be orthogonal with respect to the joint probability of these random variables:

$$\langle \psi_i \psi_j \rangle = \frac{1}{\sqrt{2\pi}} \int_{-\infty}^{\infty} \psi_k(\xi)\psi_k(\xi)\rho(\xi)d\xi = \delta_{ij}\langle \psi_i^2 \rangle \quad (48)$$

where u_i are deterministic coefficients, referred to as PC coefficients.

Wiener in his original article (1938) considered the spectral representation of random variables by Hermite polynomial with germs as Gaussian random variables. The PCE was later generalised by D. Xiu, et al. (2002) [12] known as generalised Polynomial chaos or gPC. Table 1 mentions the polynomial type and its corresponding random variable or germ.

Table 1. Generalised polynomial chaos (adapted from [12]).

Uncertain parameter type	Optimal polynomial type
Gaussian	Hermite
Gamma	Laguerre
Beta	Jacobi
Uniform	Legendre

In this article, Gauss-Hermite PCE type has been considered, and the basis functions are Hermite polynomials as a function of Gaussian random variables ξ.

In order to obtain the deterministic coefficient u_i, the random variable u is projected on to the space spanned by Hermite polynomials as its basis. The number of degrees of freedom of the random variables determines the dimension of the germ ξ. However, if the random variable has infinite degrees of freedom, then in that case the number of terms (T) after which the KKL expansion is truncated determines the dimensionality of ξ. Given the space dimension T (number of random variables) and the order of the polynomial chaos p, a basis dimension P containing the number of PC used in the expansion can be computed as [18, 37]:

$$P + 1 = \frac{(T + p)!}{p! \, T!}$$

where p depends on the information contained about the random variable that has been represented. Table 2 shows the number of terms of P for a given truncation T and order of polynomial p. If the truncation order T is 3 and the order of polynomial is 1, P=5. If the truncation order T is 5 and the order of the polynomial is 2, then P=20.

Table 2. Hermite polynomial chaos in 1D and 2D (adapted from R.G. Ghanem, et al. (2012) [10]).

Order p	1D		2D	
	Index k	PC ($\Psi_k(\xi_1)$)	Index k	PC ($\Psi_k(\xi_1,\xi_2)$)
0	0	1	0	1
1	1	ξ_1	1	ξ_1
			2	ξ_2
2	2	$\xi_1^2 - 1$	3	$\xi_1^2 - 1$
			4	$\xi_1\xi_2$
			5	$\xi_2^2 - 1$
3	3	$\xi_1^3 - 3\xi_1$	6	$\xi_1^3 - 3\xi_1$
			7	$\xi_1^2\xi_2 - \xi_2$
			8	$\xi_1\xi_2^2 - \xi_1$
			9	$\xi_2^3 - 3\xi_2$
4	4	$\xi_1^4 - 6\xi_1^2 + 3$	10	$\xi_1^4 - 6\xi_1^2 + 3$
			11	$\xi_1^3\xi_2 - 3\xi_1\xi_2$
			12	$\xi_1^2\xi_2^2 - \xi_1^2 - \xi_2^2 + 1$
			13	$\xi_1\xi_2^3 - 3\xi_1\xi_2$
			14	$\xi_2^4 - 6\xi_2^2 + 3$
5	5	$\xi_1^5 - 10\xi_1^3 + 15\xi_1$	15	$\xi_1^5 - 10\xi_1^3 + 15\xi_1$
			16	$\xi_1^4\xi_2 - 6\xi_1^2\xi_2 + 3\xi_2$
			17	$\xi_1^3\xi_2^2 - \xi_1^3 - 3\xi_1\xi_2^2 + 3\xi_1$
			18	$\xi_1^2\xi_2^3 - \xi_2^3 - 3\xi_1^2\xi_2 + 3\xi_2$
			19	$\xi_1\xi_2^4 - 6\xi_1\xi_2^2 + 3\xi_1$
			20	$\xi_2^5 - 10\xi_2^3 + 15\xi_2$

The equation of motion of a free vibration of a beam can be written as:

$$[M]\{\ddot{u}\} + [K]\{u\} = 0$$

Now, uncertainty in the modulus of elasticity will result in uncertainty in the stiffness matrix (K) such that:

$$K_i(\xi) = K_0 + \sum_{i=1}^{M} K_i\xi_i(\theta) \quad (49)$$

Since uncertainty in K will induce uncertainty in u, a polynomial chaos expansion for u is specified:

$$u = \sum_{k=0}^{\infty} u_k\psi_k(\xi) \quad (50)$$

where u_k is a deterministic unknown coefficient.

The eigenvalue equation of the vibration of a beam can be written as:

$$(K - \lambda \mathcal{M})u = 0 \quad (51)$$

Substituting the value of u and K in Eq. (51), we obtain:

$$\left\{ \left(K_0 + \sum_{i=1}^{T} K_i\xi_i \right) - M\lambda \right\} \left\{ \sum_{j=1}^{P} u_{n_i}\langle \psi_j \rangle \right\} = 0 \quad (52)$$

Multiplying both sides of the equation with ψ_k, and taking the expectation with respect to the basis germ ξ, we obtain:

$$\sum_{i=0}^{T}\sum_{j=1}^{P}\sum_{k=1}^{P} K_i u_{n_j} \langle \xi_i \psi_j \psi_k \rangle - M \sum_{j=1}^{P}\sum_{k=1}^{P} u_{n_j} \lambda \langle \psi_j \psi_k \rangle \quad (53)$$

Taking $u(n_j)$ common, we obtain:

$$\left(\sum_{i=0}^{T}\sum_{j=1}^{P}\sum_{k=1}^{P} K_i \langle \xi_i \psi_j \psi_k \rangle - M(\sum_{j=1}^{P}\sum_{k=1}^{P} \lambda \langle \psi_j \psi_k \rangle) \right) u_{n_j} = 0 \quad (54)$$

Substituting $\langle \xi_i \psi_j \psi_k \rangle = e_{ijk}$, we obtain:

$$\left(\sum_{i=0}^{T}\sum_{j=1}^{P}\sum_{k=1}^{P} K_i e_{ijk} - M(\sum_{j=1}^{P}\sum_{k=1}^{P} \lambda \langle \psi_j \psi_k \rangle) \right) u_{n_j} = 0 \quad (55)$$

where

$$e_{ijk} = E[\xi_i \psi_j \psi_k] = \frac{1}{\sqrt{2\pi}} \int_{-\infty}^{\infty} \xi_i \psi_j(\xi) \psi_k(\xi) \rho(\xi) d\xi \quad (56)$$

The assembly of the stiffness matrix K is given in Refs. [38] and [39] as:

$$\mathcal{K} = \sum_{i=0}^{T} K_i \otimes e_{ijk} \quad (57)$$

where $\otimes$ denotes the Kronecker product. Finally, K can be represented as:

$$\begin{bmatrix} \sum_{i=0}^{T} K_i e_{i11} & \cdots & \sum_{i=0}^{T} K_i e_{i1P} \\ & \cdots & \\ & \cdots & \\ \sum_{i=0}^{T} K_i e_{iP1} & \cdots & \sum_{i=0}^{T} K_i e_{iPP} \end{bmatrix} \quad (58)$$

The assembly of mass matrix M is given in Ref. [39] as:

$$\mathcal{M} = M \otimes e_{0jk} \quad (59)$$

and

$$\lambda^T = [\lambda_1 \ \cdots \ \lambda_P]^T \quad (60)$$

where M is the mass matrix and λ is the eigen value.

The mean (m_U) and variance of the PC expansion can be given by Eq. (61) and Eq. (62), respectively, as:

$$m_U = \int \sum_{p=0}^{P} \lambda_P \psi_p(\xi) \rho(\xi) d(\xi) = \lambda_1 \quad (61)$$

$$\text{Variance} = \int \left[\sum_{p=1}^{P} \lambda_P \psi_p(\xi) - \lambda_1 \right]^2 \rho(\xi) d(\xi) \quad (62)$$

2.5. Random sampling method

In the RSM for a given mean and standard deviation of the elastic modulus, one can randomly choose a vector of size *n* assuming normal distribution. Using these *n* values of elastic modulus, for all possible combinations, the structural dynamic characteristics of the beam is evaluated. For example, if the beam is divided into two elements, then each element can have one value of elastic modulus. Considering E_1 and E_2 as two possible values of elastic modulus, the possible combinations are [E_1E_1, E_1E_2, E_2E_1, E_2E_2]. Similarly, for N elements with N possible values of elastic modulus, the total number of combinations will be N^N. It may be noted that the total number of possible cases increases rapidly with number of elements of the beam. For ten elements, the number of possible combinations is 10^{10}.

Figure 12 illustrates the convergence plots of the first three eigenfrequencies as a function of the number of elements. In Figs. 12A and 12B, it is evident that the first two natural frequencies converge satisfactorily with five elements. However, Fig. 12C reveals that achieving convergence for the third frequency necessitates at least six elements.
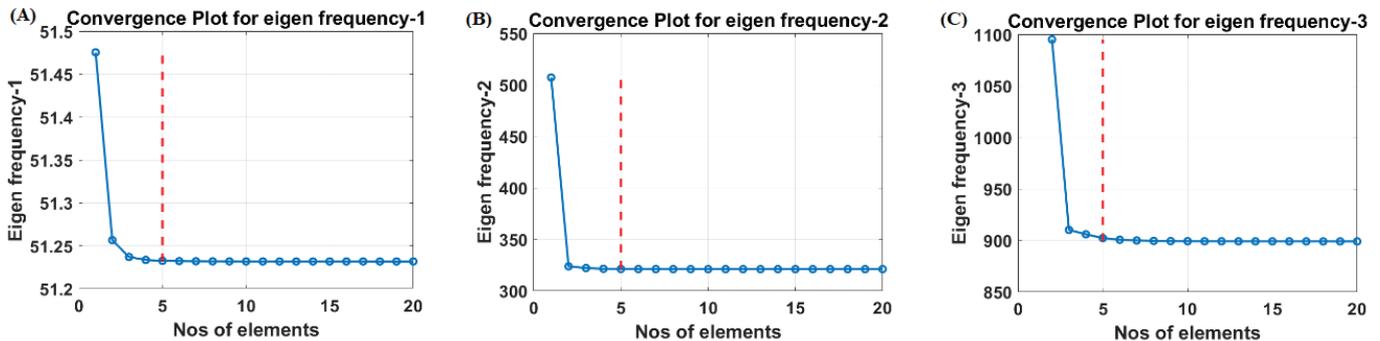

Fig. 12. Convergence plot of eigenfrequencies with number of finite elements.

The computational cost, particularly for the RSM, exhibits an exponential increase with the number of elements, escalating from 3125 to 46656 evaluations. This steep rise poses a significant challenge for practical implementation, highlighting the need for a balanced approach.

To strike a compromise between accuracy and computational cost, this paper adopts five elements for RSM and six elements for MCS-CD, MCS-KKL, and PCE methods. This decision is made to optimise computational efficiency while ensuring sufficient accuracy for reliable analysis.

By implementing this approach, the study aims to achieve a practical balance, enabling effective analysis of natural frequencies in uniform beams without imposing prohibitive computational burdens.

3. Results and discussion

In this study, a cantilever beam of length 1 m, width 12 mm, and depth 10 mm is taken as the sample problem. The first three natural frequencies and mode shapes are treated as the response quantities to study the effect of randomness of the elastic modulus. The density of material is 7850 kg/m^3. The mean value of modulus of elasticity (E) is taken as 200 GPa. The cantilever beam is discretised into finite elements, with each element having two nodes. The nodal degrees of freedom represent the nodal displacement and rotation. Cubic Hermite polynomials are used as interpolating functions between the two nodes.

In this study, the beam has been discretised into five elements for RSM and six for the other two methods. For MCS, a sample size of 2000 sets is generated. It may be noted that the mean and variance converge after a sample size of 1500 sets.
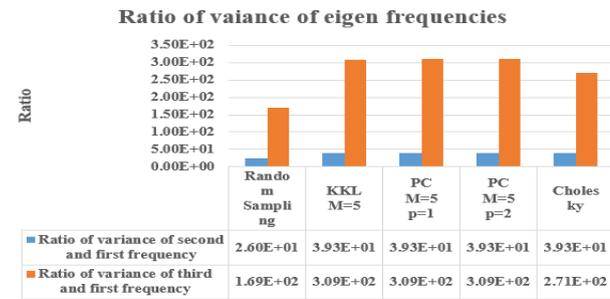
Table 3. Mean of eigenfrequencies.

Eigenfrequency in rad/sec	Random sampling	KKL M=5	PC M=5 p=1	PC M=5 p=2	Cholesky
First eigenfrequency	5.12E+01	5.12E+01	5.12E+01	5.12E+01	5.12E+01
Second eigenfrequency	3.21E+02	3.21E+02	3.21E+02	3.21E+02	3.21E+02
Third eigenfrequency	9.01E+02	9.01E+02	9.00E+02	9.00E+02	9.01E+02

Table 4. Variance of eigenfrequencies.

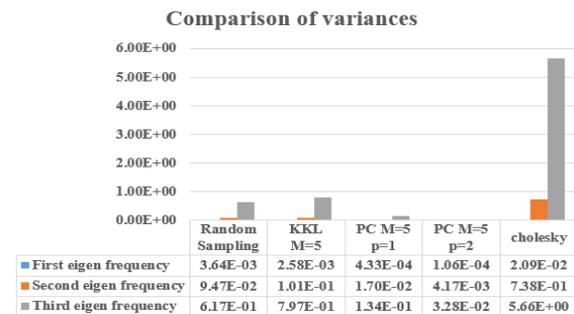| Variance of eigenfrequencies	Random sampling	KKL M=5	PC M=5 p=1	PC M=5 p=2	Cholesky
First eigenfrequency	3.64E-03	2.58E-03	4.33E-04	1.06E-04	2.09E-02
Second eigenfrequency	9.47E-02	1.01E-01	1.70E-02	4.17E-03	7.38E-01
Third eigenfrequency	6.17E-01	7.97E-01	1.34E-01	3.28E-02	5.66E+00
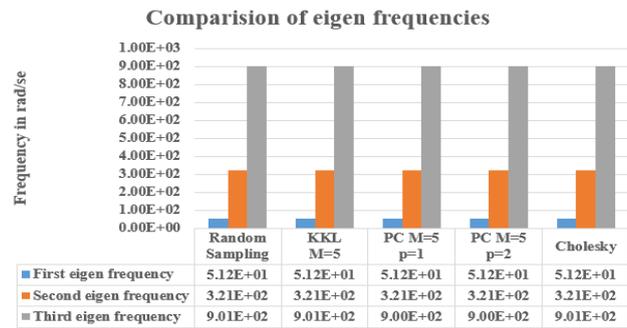
Fig. 13. Comparison of mean of eigenfrequency by Random Sampling method, Kosambi-Karhunen-Loève expansion, Polynomial Chaos expansion, and Monte Carlo simulations with Cholesky decomposition.

Fig. 14. Comparison of ratio of variance of third and second eigenfrequency with first eigenfrequency.

Figure 13 illustrates that all four methods yield nearly identical eigenfrequencies. However, there is a notable disparity in the variance among these methods. Additionally, within each method, there is a sharp increase in variance across different eigenfrequencies (Table 3). Fig. 14 highlights this observation, showing that the ratio of the variance of the third to the first eigenfrequency is approximately 100. The elevated variance of the third eigenfrequency holds significant implications, particularly considering its crucial role in the vibration characteristics of rotor blades.
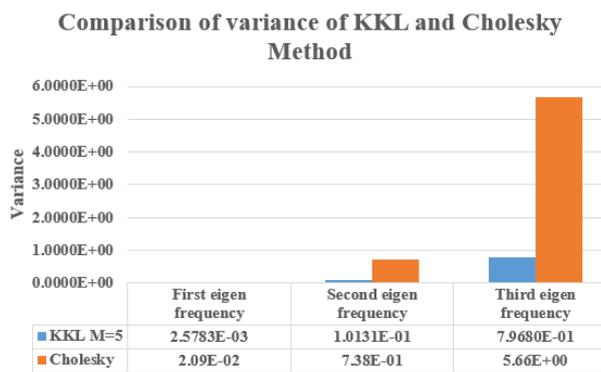

Fig. 15. Comparison of variance of eigenfrequency by Random Sampling method, Kosambi-Karhunen-Loève expansion, Polynomial Chaos expansion, and Monte Carlo simulations with Cholesky decomposition (Table 4).

From Fig. 15, it can be observed that PCE has least variance whereas (MCS-CD) has highest variance. The observed difference in variances between polynomial chaos and MCS-CD can be attributed to the inherent characteristics of each method in handling uncertainty.

Polynomial chaos expansion systematically represents the uncertain input variables (in this case, random elastic modulus) as a series of orthogonal polynomials, allowing for efficient and accurate estimation of the response statistics. This method excels in capturing the variability in the system with a reduced number of simulations, leading to a lower variance in the results. Essentially, polynomial chaos provides a more focused and structured approach to handle uncertainty.

On the other hand, MCS-CD rely on random sampling and, in certain scenarios, may encounter challenges, such as the occurrence of outliers. These anomalies can lead to significant variations in the results, resulting in higher variances. Cholesky decomposition, particularly when applied to normal distributions with specific covariance conditions, might introduce instabilities that contribute to the increased variance observed in the eigenfrequency estimates.
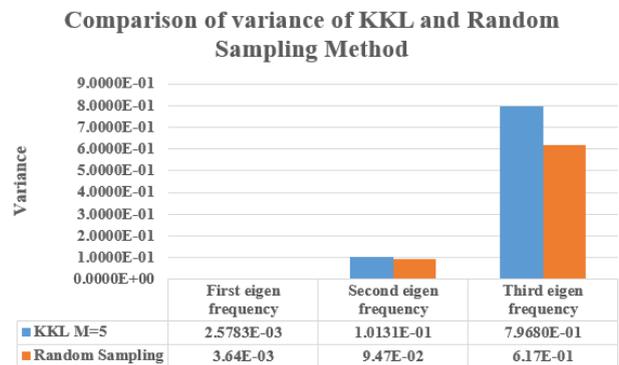

Fig. 16. Comparison of variance of eigenfrequency by Monte Carlo simulations with Cholesky decomposition and Monte Carlo simulations with Kosambi-Karhunen-Loève expansion.

Similarly, from Fig. 16, it can be observed that MCS-CD has higher variance compared to MCS-KKL. The observed difference in variances between MCS using the KKL expansion method and MCS-CD can be attributed to the specific characteristics and advantages of the KKL expansion approach in handling uncertainty.

KKL expansion is a technique that efficiently represents a random field in terms of uncorrelated modes. These modes capture the major variations in the random field, allowing

for a more effective dimensionality reduction. When applied to MCS, the KKL expansion method effectively captures the dominant modes of variability in the elastic modulus field, leading to a more focused and reduced set of samples needed for estimation.

On the other hand, Cholesky decomposition involves transforming a covariance matrix to obtain uncorrelated samples. In certain situations, particularly when the covariance structure is intricate or when dealing with specific distributions, Cholesky decomposition may lead to challenges, including potential numerical instabilities. These challenges can contribute to a broader spread of samples and, consequently, a higher variance in the results compared to the KKL expansion method.

Fig. 17. Comparison of variance of eigenfrequency by Monte Carlo simulations with Kosambi-Karhunen-Loève expansion and Random Sampling method.

From Fig. 17, it can be observed that RSM and MCS-KKL have nearly identical variance. The similarity in variance between the proposed RSM and KKL expansion can be explained by their shared focus on efficiently representing and exploring the dominant modes of variability in the system. Both methods aim to capture the key patterns in the random field, allowing for a more focused analysis and reducing the overall variability in the results.

Similarly, the reason that RSM has lower variance as compared to MCS-CD is that the permutation-based nature of RSM introduces a level of variability, particularly when exploring a wide range of possible combinations. In contrast, MCS with Cholesky can face challenges related to numerical instability and negative modulus values, potentially leading to a broader spread of samples and higher variance.

Comparing the variance of RSM with PCE, it can be observed that RSM has higher variance. This can be attributed to the fact that Polynomial chaos relies on structured representations using orthogonal polynomials,
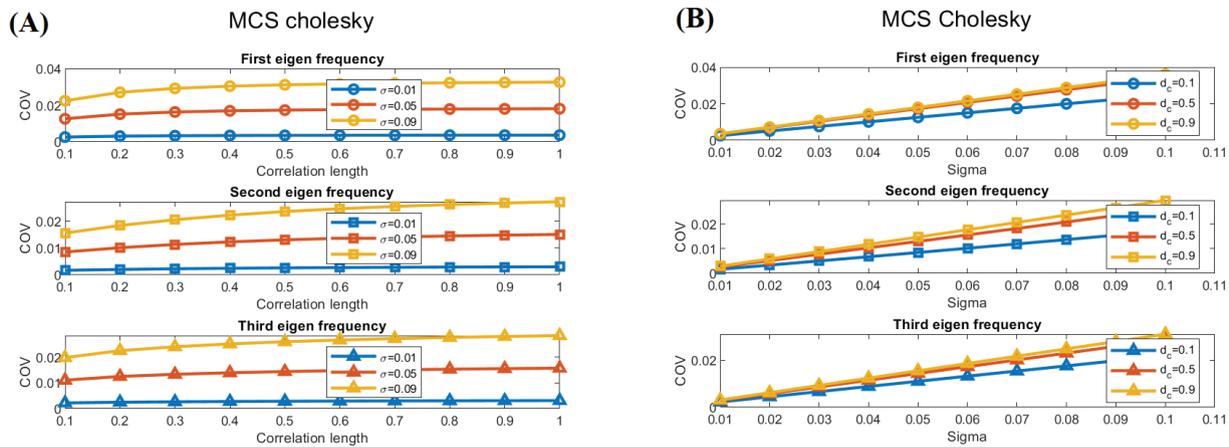
Fig. 18. COV of eigenfrequencies with correlation length and sigma for normal distribution.
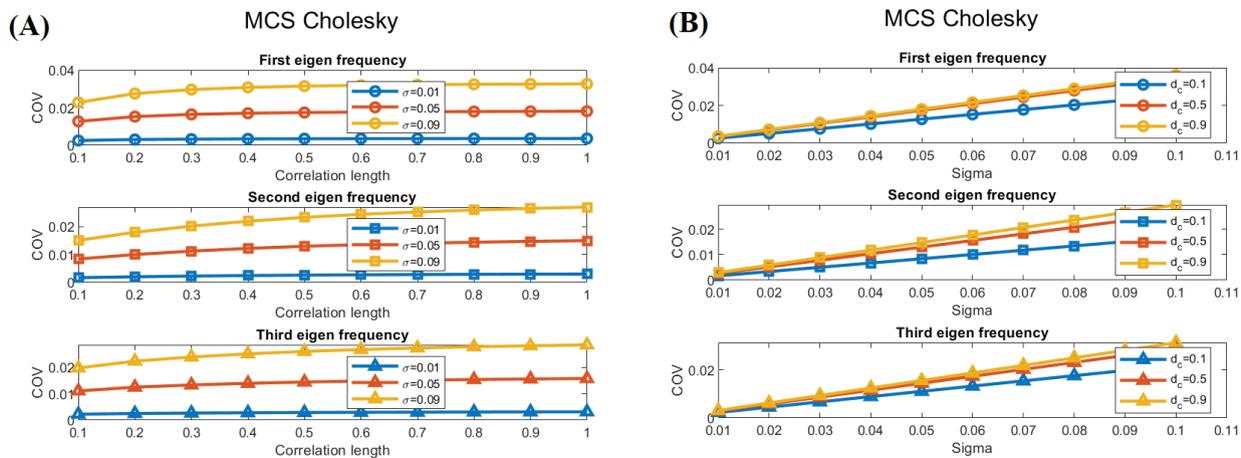

Fig. 19. COV of eigenfrequencies with correlation length and sigma for lognormal distribution.

contributing to a more controlled and focused analysis, resulting in lower variances. RSM, while comprehensive in exploration, may introduce more variability due to its unstructured permutation-based nature.

Figure 18A displays the variation of the COV of eigenfrequencies with correlation length for different values of sigma, while Fig. 18B depicts the variation of COV with sigma for different values of correlation length. These analyses were conducted using MCS-CD for both normally distributed elastic modulus. Similarly, Fig. 19A displays the variation of the COV of eigenfrequencies with correlation length for different values of sigma, while Fig. 19B depicts the variation of COV with sigma for different values of correlation length for log normally distributed elastic modulus for MCS-CD. It can be observed that both normal and lognormal distribution of elastic modulus give similar results. This can be reasoned because the transformation from a normal distribution to a lognormal distribution involves an exponential function. It is possible that the transformation of the random variable by the exponential function cancels out terms of the covariance of the response. Also, the statistical properties of the normal and lognormal distributions are different, but when we compute the covariance of the response, the specific transformation might lead to similar results. The correlation structure and variability may be preserved even after the distribution change.

Figure 20A displays the variation of the COV of eigenfrequencies with correlation length for different values of sigma, while Fig. 20B depicts the variation of COV with sigma for different values of correlation length. These analyses were conducted using MCS-KKL for both normally-distributed elastic moduli. Similarly, Fig. 21A displays the variation of the COV of eigenfrequencies with correlation length for different values of sigma, while Fig. 21B depicts the variation of COV with sigma for different
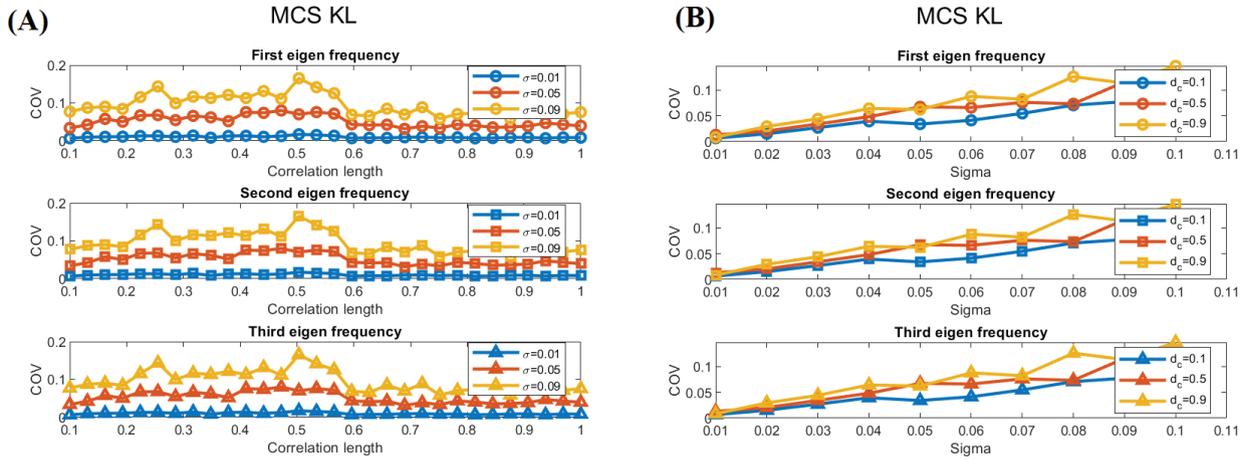
Fig. 20. COV of eigenfrequencies with correlation length and sigma for normal distribution.
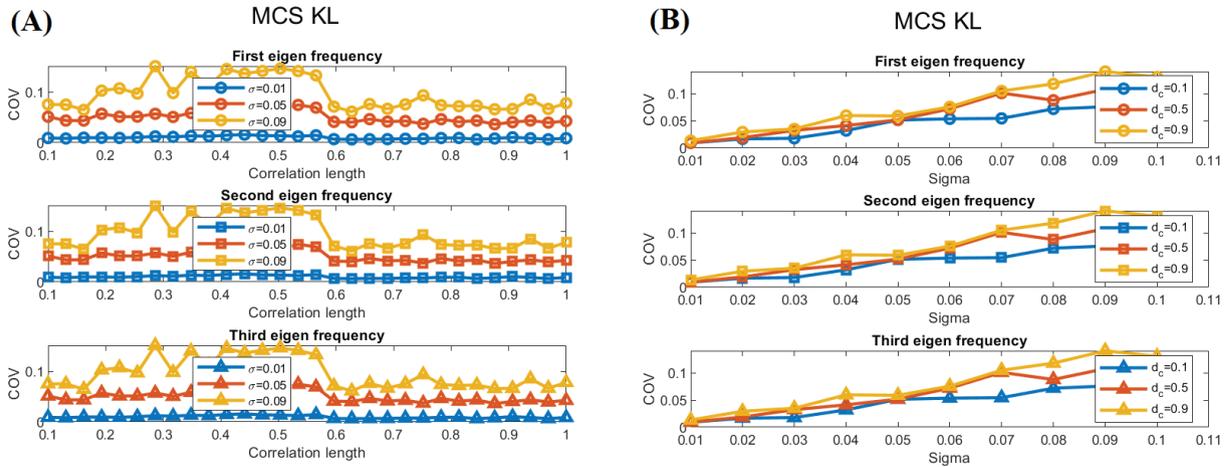

Fig. 21. COV of eigenfrequencies with correlation length and sigma for lognormal distribution.

values of correlation length for lognormally distributed elastic moduli for MCS-KKL. In this case, normal and lognormal distributions do not have any significant effect on the COV of the response. This can be attributed to the fact that MCS methods such as Cholesky decomposition and KKL expansion may be less sensitive to the choice of distribution for certain types of problems. The algorithms used in these methods could handle the transformation without significantly impacting the covariance of the response. The correlation length and the correlation structure of the random elastic modulus may have a more dominant effect on the covariance of the response than the specific choice between a normal and lognormal distribution.

Figure 22A displays the variation of the COV of Eigenfrequencies with correlation length for different values of sigma, while Fig. 22B depicts the variation of COV with sigma for different values of correlation length. These analyses were conducted using PCE for normally

distributed elastic modulus. Similarly, Fig. 23A displays the variation of the COV of eigenfrequencies with correlation length for different values of sigma, while Fig. 23B depicts the variation of COV with sigma for different values of correlation length for log normally distributed elastic modulus for PCE. In this case, the COV of response varies significantly for normal and lognormal distribution. This can happen because PCE relies on orthogonal polynomials as the basis functions. These polynomials are specifically designed to work well with certain types of distributions. If the distribution changes from normal to lognormal, the orthogonality properties of the polynomial basis may be affected, leading to different behaviours in the PCE. Also, PCE involves the expansion of the response in terms of orthogonal polynomials of the random variables. The transformation of the random variable from a normal to a lognormal distribution involves different mathematical operations (exponential function), and this transformation can affect the representation of the response in the PCE.
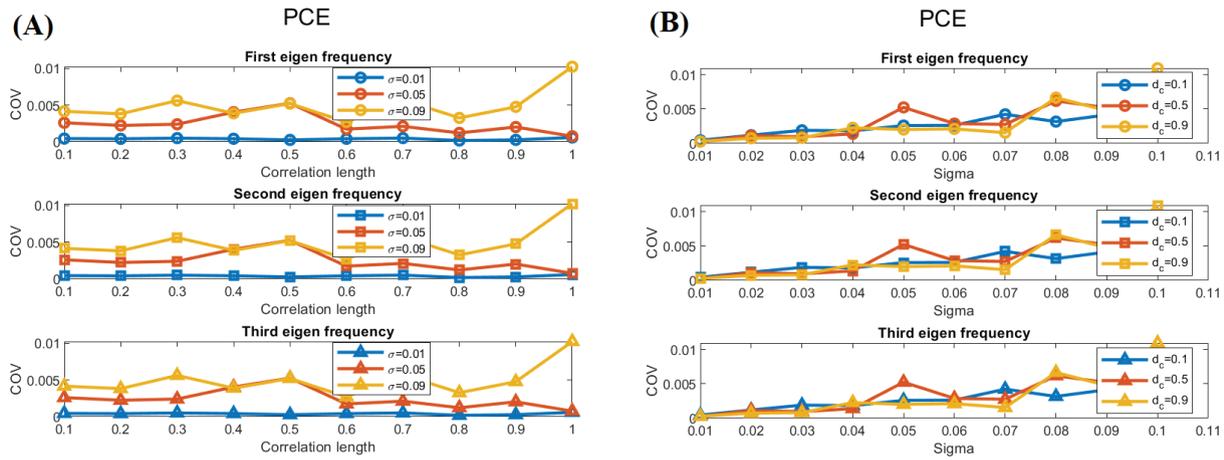
Fig. 22. COV of eigenfrequencies with correlation length and sigma for normal distribution.
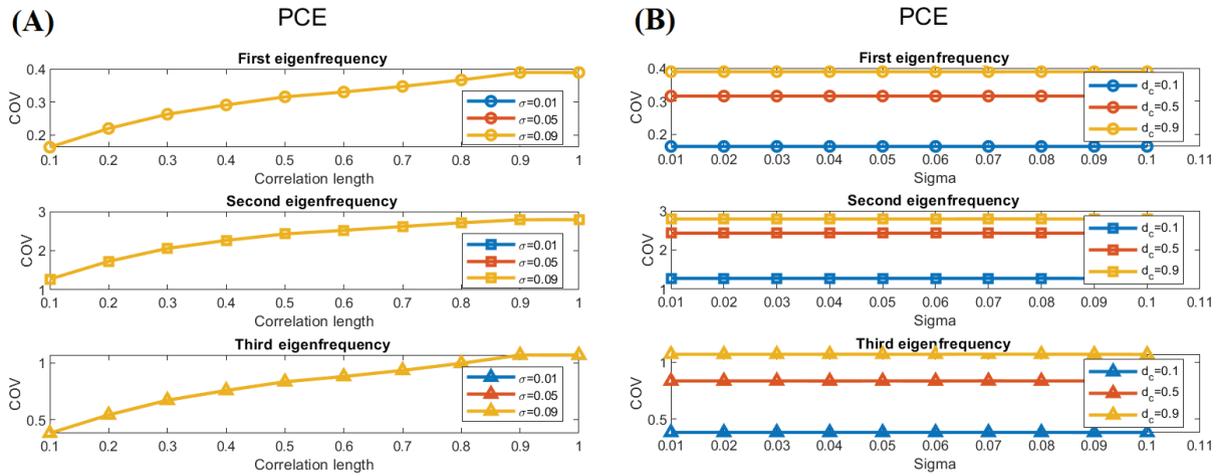

Fig. 23. COV of eigenfrequencies with correlation length and sigma for lognormal distribution.

Table 5. Computational cost.

Method	Number of simulations	Computational time (in seconds)
MCS-CD	2000	19.95792
MCS-KKL	2000	1.312695
PCE (T=5, p=1)	5	0.017394
PCE (T=5, p=2)	20	0.03018
RSM (nos. of elements=5)	3125	31.63806

Table 5 provides a comparison of the computational cost for different RSMs including MCS-CD, MCS-KKL, PCE with different polynomial orders, and RSM.

The computational cost for RSM is relatively higher compared to MCS-CD, MCS-KKL and PCE. This can be attributed to the nature of RSM, which involves evaluating the structural dynamic characteristics of the beam for all possible combinations of elastic modulus values.

Despite requiring a larger number of simulations compared to other methods, RSM provides a comprehensive analysis by considering all possible combinations of elastic modulus values, this exhaustive approach ensures a thorough exploration of the structural behaviour under varying material properties.

MCS-KKL demonstrates lower computational cost compared to MCS with MCS-CD, suggesting that MCS-KKL may be a more efficient RSM for the given analysis. KKL offers optimised sampling strategies that lead to faster convergence and reduced computational cost. It leverages the eigenstructure of the covariance matrix to efficiently sample from the underlying distribution, resulting in fewer iterations required to achieve accurate results compared to traditional methods like Cholesky decomposition.

It may be noted that RSM may require more computational resources due to the exponential increase in possible combinations with the number of elements, it offers a comprehensive analysis of the structural behaviour, which can be valuable for understanding the effects of material variability on the system response.

Figure 24 depicts the mode shapes of MCS-CD, MCS-KKL, RSM, and PCE. Upon examination of Figs. 24A and 24B, it becomes apparent that the spread of mode shapes in MCS-CD is larger compared to the proposed RSM and MCS-KKL. Furthermore, the spread of mode shapes in MCS-KKL and RSM appears to be nearly identical. This difference can be attributed to variations in their respective variances. The observed differences in the spread of mode shapes among MCS-CD, MCS-KKL, RSM, and PCE models bear practical significance in structural design and analysis. Understanding the variations in mode shapes can provide valuable insights into the dynamic behaviour of the system under consideration. For instance, a larger

spread of mode shapes, as seen in MCS-CD, may indicate increased uncertainty or variability in structural response, necessitating robust design strategies. Conversely, the similarity in mode shapes between MCS-KKL and RSM suggests a comparable predictive capability between these methods, offering potential efficiency gains in computational modelling and analysis tasks.

4. Conclusions

In this study, we have thoroughly investigated the influence of random elastic modulus on beam eigenfrequencies using various simulation techniques, including MCS-CD and MCS-KKL, PCE, and a proposed RSM. We successfully addressed anomalies encountered in MCS by adopting a log-normal distribution for the elastic modulus, effectively mitigating negative values and imaginary eigenfrequencies. Through comparative analyses focusing on covariance variation of the first three eigenfrequencies with correlation length and standard
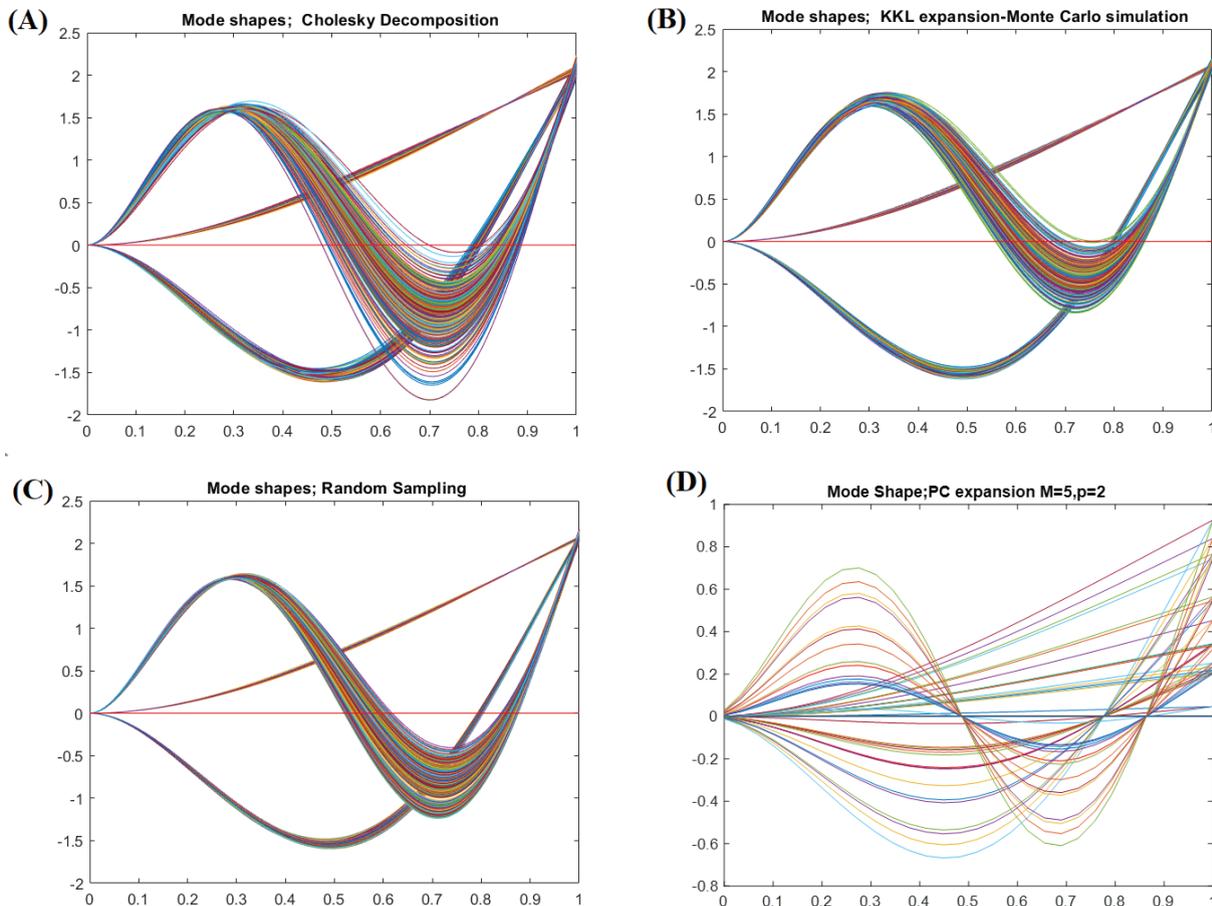

Fig. 24. Mode shapes for Monte Carlo simulations with Cholesky decomposition, Monte Carlo simulations with Kosambi-Karhunen-Loève expansion, Random Sampling method and Polynomial Chaos expansion.

deviation of the random field, we highlighted nuanced differences between normal and log-normal distributions. Additionally, PCE revealed distinct responses, showcasing variations in covariance with different distributions.

Our study culminated in eigenfrequency estimation using the proposed RSM, where the beam was discretised into n elements with randomly assigned elastic moduli. Comparative analysis with existing methods showed that the RSM yields nearly identical results for small numbers of finite elements, with the variance of the proposed method closely approximating that of the KKL method. However, it is essential to note that the proposed method becomes computationally expensive as the number of elements increases. For instance, when the number of elements increases from n=6 to n=7, the computational complexity rises significantly from 6^6=46,656 to 7^7=823,543. Therefore, while the RSM offers promising results, its scalability may pose challenges in computational resources for larger structural models.

ACKNOWLEDGEMENTS

COMPETING INTERESTS

The author declares that there is no conflict of interest regarding the publication of this article.

REFERENCES

[1] K.M. Hamdia, H. Ghasemi (2022), "Quantifying the uncertainties in modeling soft composites via a multiscale approach", *Int. J. Solids Struct.*, **256(5)**, DOI: 10.1016/J.IJSOLSTR.2022.111959.

[2] H. Khakurel, M.F.N. Taufique, A. Roy, et al. (2021), "Machine learning assisted prediction of the Young's modulus of compositionally complex alloys", *Sci. Reports*, **11(1)**, DOI: 10.1038/s41598-021-96507-0.

[3] C. Soyarslan, M. Pradas, S. Bargmann (2019), "Effective elastic properties of 3D stochastic bicontinuous composites", *Mech. Mater.*, **137**, DOI: 10.1016/j.mechmat.2019.103098.

[4] P.C. Nguyen, T.N. Van, H.T. Duy (2022), "Stochastic free vibration analysis of beam on elastic foundation with the random field of Young's modulus using finite element method and Monte Carlo simulation", *Lect. Notes Civ. Eng.*, Springer, pp.499-506, DOI: 10.1007/978-981-16-7160-9_50.

[5] A. Farsi, A.D. Pullen, J.P. Latham, et al. (2017), "Full deflection profile calculation and Young's modulus optimisation for engineered high performance materials", *Sci. Reports*, **7**, DOI: 10.1038/srep46190.

[6] T.D. Hien, M. Kleiber (1990), "Finite element analysis based on stochastic Hamilton variational principle", *Comput. & Struct.*, **37(6)**, pp.893-902, DOI: 10.1016/0045-7949(90)90002-J.

[7] X.L. Liu, C.S. Oliveira (2003), "Iterative modal perturbation and reanalysis of eigenvalue problem", *Commun. Numer. Methods Eng.*, **19(4)**, pp.263-274, DOI: 10.1002/cnm.587.

[8] W.K. Liu, T. Belytschko, A. Mani (1986), "Probabilistic finite elements for nonlinear structural dynamics", *Comput. Methods in Appl. Mech. and Eng.*, **56(1)**, pp.61-81, DOI: 10.1016/0045-7825(86)90136-2.

[9] R. Ghanem, P.D. Spanos (1990), "Polynomial chaos in stochastic finite elements", *J. Appl. Mech.*, **57(1)**, pp.197-202, DOI: 10.1115/1.2888303.

[10] R.G. Ghanem, P.D. Spanos (2012), *Stochastic Finite Element: A Spectral Approach*, Springer, 240pp.

[11] D. Lucor, G.E. Karniadakis (2004), "Adaptive generalised polynomial chaos for nonlinear random oscillators", *SIAM J. Sci. Comput.*, **26(2)**, DOI: 10.1137/S1064827503427984.

[12] D. Xiu, G.E. Karniadakis (2002), "The Wiener-Askey polynomial chaos for stochastic differential equations", *SIAM J. Sci. Comput.*, **24(2)**, pp.619-644, DOI: 10.1137/S1064827501387826.

[13] M. Papadrakakis, V. Papadopoulos (1996), "Robust and efficient methods for stochastic finite element analysis using Monte Carlo simulation", *Comput. Methods in Appl. Mech. and Eng.*, **134(3-4)**, pp.325-340, DOI: 10.1016/0045-7825(95)00978-7.

[14] L. Wang (2008), *Karhunen-Loeve Expansions and Their Applications*, London School of Economics and Political Science (United Kingdom), 292pp.

[15] M. Eiermann, O.G. Ernst, E. Ullmann (2007), "Computational aspects of the stochastic finite element method", *Comput. Vis. Sci.*, **10**, pp.3-15, DOI: 10.1007/s00791-006-0047-4.

[16] K.K. Phoon, S.P. Huang, S.T. Quek (2002), "Implementation of Karhunen-Loeve expansion for simulation using a wavelet-Galerkin scheme", *Probabilistic Eng. Mech.*, **17(3)**, pp.293-303, DOI: 10.1016/S0266-8920(02)00013-9.

[17] S.P. Huang, S.T. Quek, K. Phoon (2001), "Convergence study of the truncated Karhunen-Loeve expansion for simulation of stochastic processes", *Int. J. Numer. Methods Eng.*, **52(9)**, pp.1029-1043, DOI: 10.1002/nme.255.

[18] P.D. Spanos, R. Ghanem (1989), "Stochastic finite element expansion for random media", *J. Eng. Mech.*, **115(5)**, DOI: 10.1061/(ASCE)0733-9399(1989)115:5(1035).

[19] W. Betz, I. Papaioannou, D. Straub (2014), "Numerical methods for the discretization of random fields by means of the Karhunen-Loève expansion", *Comput. Methods in Appl. Mech. and Eng.*, **271**, pp.109-129, DOI: 10.1016/j.cma.2013.12.010.

[20] R. Ghanem, D. Ghosh (2007), "Efficient characterization of the random eigenvalue problem in a polynomial chaos decomposition", *Int. J. for Numer. Methods in Eng.*, **72(4)**, pp.486-504, DOI: 10.1002/nme.2025.

[21] B. Pascual, S. Adhikari (2012), "Hybrid perturbation-polynomial chaos approaches to the random algebraic eigenvalue problem", *Comput. Methods in Appl. Mech. and Eng.*, **217-220**, pp.153-167, DOI: 10.1016/j.cma.2012.01.009.

[22] S.B. Mulani, R.K. Kapania, R.W. Walters (2006), "Stochastic eigenvalue problem with polynomial chaos", *47ᵗʰ AIAA/ASME/ASCE/AHS/ASC Structures, Structural Dynamics, and Materials Conference*, DOI: 10.2514/6.2006-2068.

[23] C.V. Verhoosel, M.A. Gutiérrez, S.J. Hulshoff (2006), "Iterative solution of the random eigenvalue problem with application to spectral stochastic finite element systems", *Int. J. Numer. Methods Eng.*, **68(4)**, pp.401-424, DOI: 10.1002/nme.1712.

[24] E. Sarrouy, O. Dessombz, J.J. Sinou (2012), "Stochastic analysis of the eigenvalue problem for mechanical systems using polynomial chaos expansion-application to a finite element rotor", *J. Vib. Acoust.*, **134(5)**, DOI: 10.1115/1.4005842.

[25] T.N. Van, H.C. Noh (2017), "Investigation into the effect of random material properties on the variability of natural frequency of functionally graded beam", *KSCE J. Civ. Eng.*, **21(4)**, pp.1264-1272, DOI: 10.1007/s12205-016-0012-9.

[26] B.S.L.P.D. Lima, N.F.F. Ebecken (2000), "A comparison of models for uncertainty analysis by the finite element method", *Finite Elements in Analysis and Design*, **34(2)**, pp.211-232, DOI: 10.1016/S0168-874X(99)00039-6.

[27] P. Pluch (2004), "Some theory for the analysis of random fields", *arXiv*, DOI: 10.48550/arXiv.math/0701323.

[28] S. Chakraborty, S.S. Dey (1995), "Stochastic finite element method for spatial distribution of material properties and external loading", *Comput. Struct.*, **55(1)**, pp.41-45, DOI: 10.1016/0045-7949(94)00504-V.

[29] R. Kumar (2024), "Heat transfer in material having random thermal conductivity using Monte Carlo simulation and deep neural network", *Multiscale and Multidisciplinary Modeling, Experiments and Design*, DOI: 10.21203/rs.3.rs-3828635/v1.

[30] B. Schölkopf, A.S.K.R. Müller (1998), "Nonlinear component analysis as a Kernel eigenvalue problem", *Neural Computation*, **10**, pp.1299-1319.

[31] P. Sarma, L.J. Durlofsky, K. Aziz (2008), "Kernel principal component analysis for efficient, differentiable parameterization of multipoint geostatistics", *Math. Geosci.*, **40(1)**, pp.3-32, DOI: 10.1007/s11004-007-9131-7.

[32] J.T.Y. Kwok, I.W.H. Tsang (2004), "The pre-image problem in kernel methods", *IEEE Trans. Neural Networks*, **15(6)**, pp.1517-1525, DOI: 10.1109/TNN.2004.837781.

[33] A. Alexanderian (2015), "A brief note on the Karhunen-Loève expansion", *arXiv*, DOI: 10.48550/arXiv.1509.07526.

[34] B. Engelhardt (2013), "Probabilistic machine learning: Kernels and Kernel methods", https://www.cs.princeton.edu/~bee/courses/scribe/lec_10_09_2013.pdf, accessed 16 February 2023.

[35] C. Bucher (2009), *Computational Analysis of Randomness in Structural Mechanics*, CRC Press, **3**, DOI: 10.1201/9780203876534.

[36] N.A.A. Rihan (2013), *Numerical Treatment of The Fredholm Integral Equations of The Second Kind*, PhD Thesis, An-Najah National University, Nablus, Palestine.

[37] B. Sudret, A.D. Kiureghian (2000), *Stochastic Finite Element Methods and Reliability: A State-of-The-Art Report*, Report No. UCB/SEMM-2000/08, Department of Civil & Environmental Engineering, University of California, Berkeley, 189pp.

[38] M. Schevenels, G. Lombaert, G. Degrande (2004), "Application of the stochastic finite element method for Gaussian and non-Gaussian systems", *Proceedings of ISMA 2004*, pp.3299-3314.

[39] E. Jacquelin, S. Adhikari, J.J. Sinou, et al. (2015), "Polynomial chaos expansion in structural dynamics: Accelerating the convergence of the first two statistical moment sequences", *J. of Sound and Vib.*, **356**, pp.144-154, DOI: 10.1016/j.jsv.2015.06.039.